

AvatarGen: A 3D Generative Model for Animatable Human Avatars

Jianfeng Zhang^{1*}, Zihang Jiang^{1*}, Dingdong Yang², Hongyi Xu²,
Yichun Shi², Guoxian Song², Zhongcong Xu¹, Xinchao Wang¹, Jiashi Feng²
¹National University of Singapore ²ByteDance

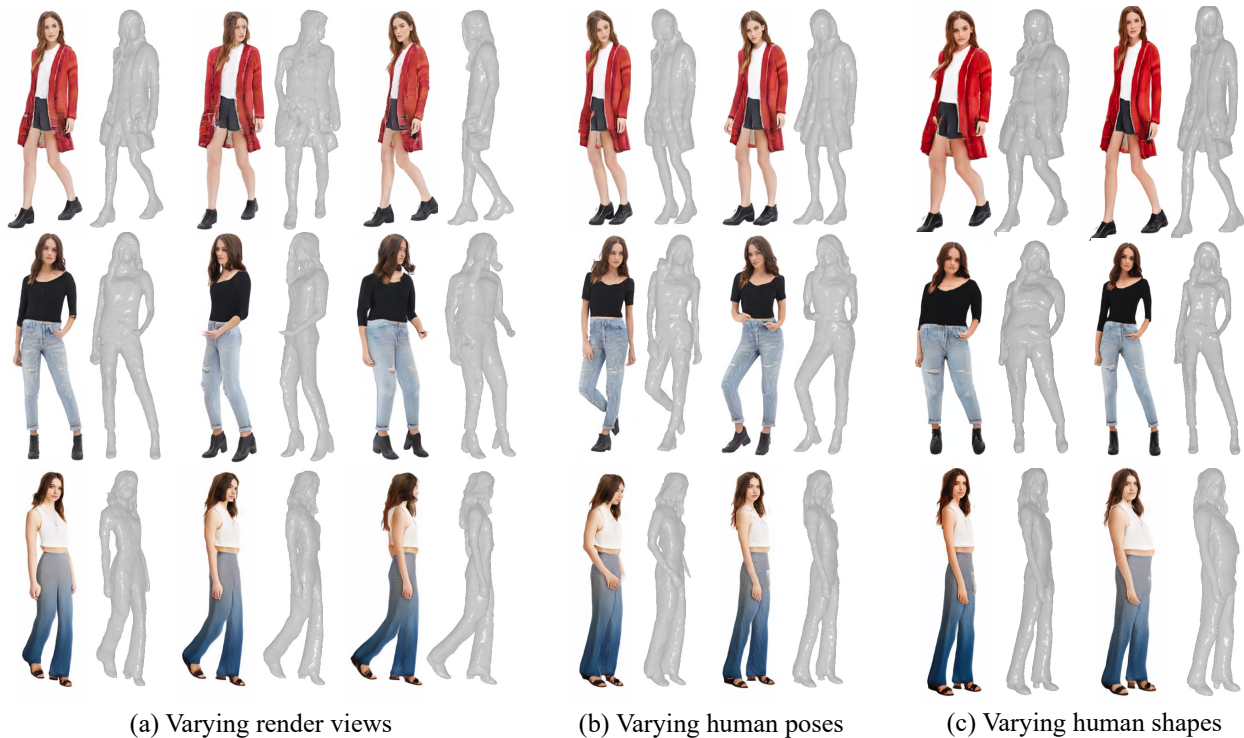


Figure 1. Our AvatarGen can synthesize clothed 3D human avatars with detailed geometries and diverse appearances under disentangled control over camera viewpoints, human poses and shapes. Please see our [project page](#) for video results.

Abstract

Unsupervised generation of 3D-aware clothed humans with various appearances and controllable geometries is important for creating virtual human avatars and other AR/VR applications. Existing methods are either limited to rigid object modeling, or not generative and thus unable to generate high-quality virtual humans and animate them. In this work, we propose AvatarGen, the first method that enables not only geometry-aware clothed human synthesis with high-fidelity appearances but also disentangled human animation controllability, while only requiring 2D images

for training. Specifically, we decompose the generative 3D human synthesis into pose-guided mapping and canonical representation with predefined human pose and shape, such that the canonical representation can be explicitly driven to different poses and shapes with the guidance of a 3D parametric human model SMPL. AvatarGen further introduces a deformation network to learn non-rigid deformations for modeling fine-grained geometric details and pose-dependent dynamics. To improve the geometry quality of the generated human avatars, it leverages the signed distance field as geometric proxy, which allows more direct regularization from the 3D geometric priors of SMPL. Benefiting from these designs, our method can generate animatable 3D

*Equal contribution.

human avatars with high-quality appearance and geometry modeling, significantly outperforming previous 3D GANs. Furthermore, it is competent for many applications, e.g., single-view reconstruction, re-animation, and text-guided synthesis/editing. Our code and models will be available at the [project page](#).

1. Introduction

Generating diverse and high-quality 3D-aware virtual humans (avatars) with precise control over their geometries, e.g., poses and shapes, is a fundamental but extremely challenging task. Solving this task will benefit many applications like immersive photography visualization [71], virtual try-on [34], VR/AR [24, 63] and image editing [21, 69].

Conventional solutions rely on classical graphics modeling and rendering techniques [7, 9, 12, 58] to create virtual avatars. Though offering high-quality, they typically require pre-captured templates, multi-camera systems, controlled studios, and long-term works of artists. In this work, we aim to make virtual human avatars widely accessible at low cost. To this end, we propose the first 3D-aware avatar generative model that can *synthesize* 1) high-quality virtual humans with 2) various appearances and disentangled geometry controllability 3) and be trainable from only 2D images, thus largely alleviating the effort to create avatars.

The 3D-aware generative models have recently seen rapid progress, fueled by introducing implicit neural representation (INR) methods [6, 38, 39, 46] into generative adversarial networks [2, 3, 17, 42, 45]. However, these models are limited to relatively simple and rigid objects, such as human faces and cars, and mostly fail to generate clothed human avatars whose appearance is highly sundry because of their articulated poses and great variability of clothing. Besides, they have limited control over the generation process and thus cannot animate the generated objects, *i.e.*, driving the objects to move by following certain instructions. Another line of works leverage INRs [39] to learn articulated human avatars for reconstructing a single subject from one’s multi-view images or videos [5, 43, 49, 50, 64]. While being animatable, these methods are *not generative* and thus cannot synthesize novel identities and appearances.

Targeting at generative modeling of animatable human avatars, we propose AvatarGen, the first model that can synthesize *novel* human avatars with disentangled control over their geometries and appearances. AvatarGen is built upon EG3D [2], a recent method that can synthesize 3D-aware human faces via introducing an effective tri-plane representation. However, it is not directly applicable for human avatar generation since it cannot handle the challenges in modeling complex textures and the articulated body structure with various poses. Moreover, EG3D has limited control ability and thus it hardly animates the generated objects.

To address these challenges, we propose to decompose the generative human avatar modeling into *pose-guided canonical mapping* and *canonical human generation*. Guided by a 3D parametric human model SMPL [36], AvatarGen un-warps each point sampled in the observation space with a specified human body to a standard avatar with predefined pose and shape, represented by tri-plane [2], in a canonical space via the inverse LBS [22]. To accommodate the non-rigid deformation between the observation and canonical spaces (like clothes wrinkle), our method further trains a deformation module to predict the proper residual deformation. As such, it can generate detailed geometry and texture for the observation space by deforming the canonical one, which is much easier to generate and shareable across different instances, thus largely alleviating the learning difficulties. Meanwhile, such decomposed formulation by design *disentangles the geometries and appearances*, offering independent control over them.

Although our method can generate 3D human avatars with reasonable geometry, we find it tends to produce noisy body surfaces due to the lack of constraints on the learned geometry (density field). Inspired by recent works on neural implicit surface [45, 50, 60, 67], we propose to use the signed distance field (SDF) to impose stronger *geometry-aware guidance* for the model training. With this, the model can leverage the prior body model to infer reasonable signed distance values, which greatly improves the quality of the human avatar generation and animation. We also introduce a local face discriminator to alleviate undesirable face generation due to low-resolution faces in the training images.

As shown in Fig. 1, trained from only 2D images, AvatarGen can synthesize a large variety of clothed human avatars with high-fidelity appearances, geometries and disentangled controllability. We evaluate AvatarGen quantitatively and qualitatively, demonstrating it strongly outperforms previous state-of-the-art methods. Moreover, our AvatarGen support several applications, like single-view 3D reconstruction, re-animation and text-guided synthesis.

2. Related Works

Generative 3D-aware image synthesis. Generative adversarial networks (GANs) [16] have recently achieved photo-realistic image synthesis [25–28]. Extending these capabilities to 3D settings has started to gain attention. Early methods combine GANs with voxel [40, 41, 62], mesh [32, 59] or point cloud [1, 31] representations for 3D-aware image synthesis. Recently, several methods represent 3D objects by learning an implicit neural representation (INR) [2, 3, 10, 17, 42, 45, 55]. Among them, some methods use INR-based model as generator [3, 10, 55], while some others combine INR generator with 2D decoder for higher-resolution image generation [17, 42, 66, 70]. Follow-up works like EG3D [2] proposes an efficient Tri-plane rep-

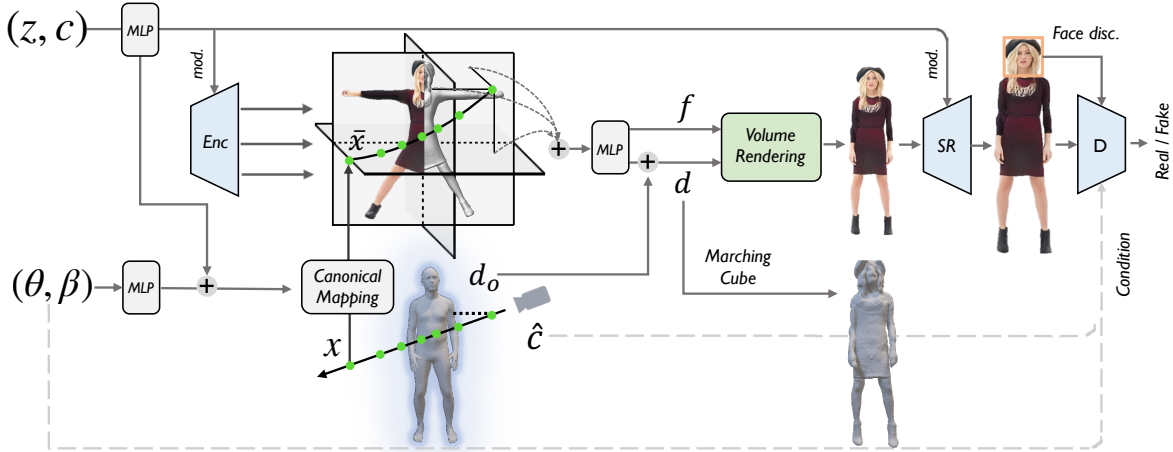


Figure 2. **Pipeline of AvatarGen.** Taking the latent code \mathbf{z} and camera pose \mathbf{c} as inputs, the encoder generates tri-plane features of a standard human avatar with canonical pose and shape. The geometry condition (θ, β) are mapped together with latent code and applied to modulate the deformation module which un-warps the sampled points \mathbf{x} from the observation space to the canonical space under the guidance of the SMPL model. The deformed positions $\bar{\mathbf{x}}$ are used to query features from the canonical tri-plane, which are then rendered as low-resolution features and images via the SDF-based volume renderer. Finally, a super-resolution module decodes the feature images to high resolution images. The generator and the discriminator with camera and geometry conditions are optimized via adversarial training.

resentation for 3D objects modeling and StyleSDF [45] replaces density field with SDF for better geometry quality. However, such methods are typically not easily extended to non-rigid humans due to complex body articulation and appearance variations. Moreover, they have limited control over the generation process, making the generated objects hardly be animated. Differently, we study the problem of 3D-aware generative modeling of clothed humans, allowing disentangled control over the geometries and appearances.

3D human reconstruction and animation. Traditional human reconstruction methods require complicated hardware that is expensive for daily use, such as depth sensors [7, 12, 58] or dense camera arrays [9, 18]. To alleviate the requirement on the capture device, some methods train neural networks to reconstruct human models from images with differentiable renderer [15, 65]. Recently, neural radiance fields (NeRF) [39] employ the volume rendering to learn density and color fields from dense camera views. Some methods augment NeRF with human body priors to enable 3D human reconstruction from sparse multi-view data [5, 51, 57, 64]. Follow-up improvements [4, 33, 49, 50, 61] are made by combining implicit representation with the SMPL model and exploiting the linear blend skinning techniques to learn animatable 3D human modeling from temporal data. However, these methods are not generative, *i.e.*, they cannot synthesize novel identities and appearances. The concurrent works ENARF-GAN [44] and EVA3D [20] also leverage 3D human priors to learn animatable 3D human GAN. However, they still suffer from undesirable artifacts and lack of precise geometry controls.

Instead, our AvatarGen achieves high-fidelity human image synthesis with disentangled geometry controllability.

3. Methodology

3.1. Overview

We introduce a 3D generative model G , named AvatarGen, that can synthesize high-quality multi-view consistent human images, with disentangled controllability on the human geometries (*e.g.*, pose and shape). It only requires 2D images for training, without using multi-view, temporal information or 3D human scan annotations.

Fig. 2 illustrates the pipeline of our proposed AvatarGen. Given a randomly sampled latent code \mathbf{z} from Gaussian distribution, conditioning camera \mathbf{c} , and a geometry parameter $\mathbf{p} = (\theta, \beta)$, where θ and β specify human pose and shape respectively, its generator G produces a 3D neural representation (*i.e.*, tri-plane [2] as detailed later) and synthesizes a photo-realistic human image $I = G(\mathbf{z}|\mathbf{c}, \mathbf{p})$ with the corresponding viewpoint, pose and shape. In this work, we use 3D parametric model SMPL [36] to represent the human geometries \mathbf{p} . Following EG3D [2], we associate each training image with a set of camera \mathbf{c} and SMPL parameters \mathbf{p} estimated from an off-the-shelf pose estimator [29].

We choose tri-plane [2] as the representation for human avatars because it is efficient and effective for high-fidelity image synthesis. The generator encodes \mathbf{z} and camera condition \mathbf{c} to a tri-plane feature field. Then given a desired camera pose $\hat{\mathbf{c}}$, a high-dimensional feature map is synthesized via querying the tri-plane features and integrating MLP-based neural radiance fields (color feature \mathbf{f} and

density σ) along the camera rays. By feeding this feature map to a super-resolution module [28], the generator produces the final image I at high resolution. We optimize G with a discriminator module D via adversarial training, resulting in view-consistent image synthesis.

To disentangle human pose and shape from appearance synthesis and achieve controllable generation, we propose a decomposition of a 3D human representation. Specifically, we model a neural human avatar in a canonical space with predefined pose and shape, while we control the final image synthesis with desired geometries by deforming the sampled rays according to the geometry parameters \mathbf{p} (Sec. 3.2). In contrast to previous works that use density fields for 3D-aware GAN [2, 17, 42], we leverage signed distance fields (SDFs) as geometry proxy, which offers more direct geometric regularization (Sec. 3.3). We optimize our generator G with a whole body and a local head discriminators via adversarial training and several carefully designed geometric regularization (Sec. 3.4).

3.2. Animatable 3D-aware Human GAN

There are two main challenges for generating 3D-aware human avatars with controllable geometries. The first is how to effectively integrate specified geometry condition \mathbf{p} into the generative model, making the generated avatar controllable and animatable. The second challenge is how to guarantee the generation quality, considering learning pose-dependent clothed human appearance and geometry is highly under-constrained and the model training is difficult. To tackle these challenges, inspired by recent dynamic neural rendering works [47, 49, 64], we propose to decompose the human avatar generation into two steps: *pose-guided canonical mapping* and *canonical human generation*.

Pose-guided canonical mapping. We define the human 2D image with SMPL \mathbf{p} as the *observation* space $\mathcal{O}(\mathbf{p})$. To relieve learning difficulties, our model attempts to deform the observation space to a *canonical* space $\mathcal{C}(\bar{\mathbf{p}})$ with a predefined template SMPL body $\bar{\mathbf{p}}$ that is shared across different identities. The deformation function $T : \mathbb{R}^3 \mapsto \mathbb{R}^3$ thus maps any spatial points \mathbf{x}_i sampled in the observation space to $\bar{\mathbf{x}}_i$ in the canonical space for volumetric rendering.

Learning such a deformation function has been proved effective for dynamic scene modeling [47, 52]. However, learning to deform in such an implicit manner cannot handle large articulation of humans and thus hardly generalizes to novel poses/shapes. To overcome this limitation, we use SMPL to explicitly guide the deformation [4, 33, 49]. SMPL defines a skinned vertex-based human model $(\mathcal{V}, \mathcal{S})$, where $\mathcal{V} = \{\mathbf{v}\} \in \mathbb{R}^{N \times 3}$ is the set of N vertices and $\mathcal{S} = \{\mathbf{s}\} \in \mathbb{R}^{N \times J}$ is a set of the skinning weights assigned for the vertex w.r.t. J joints, with $\sum_j s_j = 1, s_j \geq 0$ for every joint. With inverse LBS (IS) transformation [23], we can map the SMPL body in the observation space with pa-

rameters \mathbf{p} into the canonical space as:

$$T_{\text{IS}}(\mathbf{v}, \mathbf{s}, \mathbf{p}) = \sum_j s_j \cdot (R_j \mathbf{v} + \mathbf{t}_j), \quad (1)$$

where R_j and \mathbf{t}_j are the rotation and translation at each joint j derived from SMPL with \mathbf{p} .

This formulation can be extended to any spatial points in the observation space by adopting the same transformation from the nearest point on the surface of SMPL body [22]. Formally, for any points \mathbf{x}_i , we first find its nearest point \mathbf{v}^* on the SMPL body surface as $\mathbf{v}^* = \arg \min_{\mathbf{v} \in \mathcal{V}} \|\mathbf{x}_i - \mathbf{v}\|_2$. Then, we use the corresponding skinning weights \mathbf{s}^* to deform \mathbf{x}_i to $\bar{\mathbf{x}}'_i$ in the canonical space as:

$$\bar{\mathbf{x}}'_i = T_o(\mathbf{x}_i | \mathbf{p}) = T_{\text{IS}}(\mathbf{x}_i, \mathbf{s}^*, \mathbf{p}). \quad (2)$$

Although the SMPL-guided inverse LBS can help align the rigid skeletons with the template body, it lacks the ability to model the pose/shape-dependent deformation, like cloth wrinkles. To alleviate this issue, we further train a deformation network to learn a residual deformation that completes the fine-grained geometric deformation by

$$\Delta \bar{\mathbf{x}}_i = \text{MLPs}(\text{Concat}[\text{Embed}(\mathbf{x}_i), \mathbf{w}, \mathbf{p}]), \quad (3)$$

where \mathbf{w} is the latent style code mapped from the input latent code \mathbf{z} via MLP, which contains appearance and geometric details of the current generation. We concatenate it with the position-embedded \mathbf{x}_i and SMPL \mathbf{p} and feed them to MLPs to yield the residual deformation. Thus, the final canonical mapping T is formulated as

$$\bar{\mathbf{x}}_i = T(\mathbf{x}_i) = \bar{\mathbf{x}}'_i + \Delta \bar{\mathbf{x}}_i \quad (4)$$

Canonical human generation. After warping 3D points in $\mathcal{O}(\mathbf{p})$ back to $\mathcal{C}(\bar{\mathbf{p}})$, AvatarGen leverages the tri-plane representation for 3D-aware generation of clothed humans in the canonical space. More concretely, it first generates a canonical tri-plane via a StyleGAN backbone by taking the latent code \mathbf{z} and camera parameters \mathbf{c} as inputs. Then, for each point \mathbf{x} back-warped to $\bar{\mathbf{x}}$, the model queries the canonical tri-plane features followed by MLPs to decode color-based features \mathbf{f} and density σ for volume rendering and the following super-resolution. Note that our canonical tri-plane only needs to generate appearance and geometry with a canonical pose and shape, which alleviates the optimization difficulties and substantially helps the learning of high-quality human generation with disentangled controllability.

3.3. Geometry-aware Human Modeling

To improve geometry modeling quality of AvatarGen, inspired by recent neural implicit surface works [45, 50, 60, 67], we adopt signed distance field (SDF) instead of density

field as geometry proxy, because it introduces more direct regularizations [45, 50] and allows the model fully leverage geometric knowledge of the 3D SMPL model as guidance.

SDF prediction with geometric prior. Directly adopting SDF for clothed human modeling is non-trivial due to the complicated body articulation, pose-dependent deformation and insufficient supervisions from 2D images.

To solve these issues, we propose a simple yet effective SDF prediction scheme that fully exploits geometric priors of the SMPL body model. Specifically, given a desired SMPL parameter $\mathbf{p} = (\theta, \beta)$, we obtain its corresponding body mesh in the observation space as $M = T_{\text{SMPL}}(\mathbf{p})$, where T_{SMPL} is the SMPL transformation function. Then, for each 3D point \mathbf{x} , instead of predicting its signed distance value directly, we first compute its coarse signed distance $d_o(\mathbf{x}|\mathbf{p})$ to the closest surface point of M . Then, we feed d_o alone with the features sampled from tri-plane to a light-weight MLP to predict the *residual* signed distance Δd . The residual SDF models the fine-grained surface details, such as hairs, clothes and wrinkles that are not represented by the SMPL model (Fig. 2). The final signed distance of each point is computed as $d(\mathbf{x}|\mathbf{z}, \mathbf{c}, \mathbf{p}) = d_o + \Delta d$. Predicting SDFs on top of the coarse body mesh largely alleviating the geometry learning difficulties, thus achieving better generation and animation results. Please refer to Appendix for more details.

Moreover, despite the disentangled pipeline as illustrated in Sec. 3.2, there is no explicit loss that constrains the generated geometry to be consistent with the human pose and shape defined by \mathbf{p} . Therefore, we guide the predicted SDF d by minimizing its difference to the SDF d_o defined by the underlying SMPL body as

$$L_{\text{prior}} = \frac{1}{|R|} \sum_{\mathbf{x} \in R} w(\mathbf{x}|\mathbf{p}) \|d(\mathbf{x}|\mathbf{z}, \mathbf{c}, \mathbf{p}) - d_o(\mathbf{x}|\mathbf{p})\|, \quad (5)$$

$$w(\mathbf{x}|\mathbf{p}) = \exp\left(\frac{-d_o(\mathbf{x}|\mathbf{p})^2}{\kappa}\right).$$

Here R is the ray samples for the volume rendering, w is the weight of prior loss for point \mathbf{x} and κ is a constant scalar that defines the tightness around the surface boundary. Such a prior loss guides the generated geometry to follow the geometric attributes controlled by \mathbf{p} . We decay the weights of the geometric prior loss L_{prior} as the point moving away from the SMPL body surface, allowing higher degrees of freedom in generation of residual geometries, such as hairs and clothes.

SDF-based volume rendering. Following [45], we adopt SDF-based volume rendering to obtain the feature images. For any sampled points \mathbf{x} on the rays, we first un-warp it to $\bar{\mathbf{x}}$ by canonical mapping. We query feature $F(\bar{\mathbf{x}})$ for $\bar{\mathbf{x}}$ from the canonical tri-plane, and feed it into two MLPs to predict the color feature $\mathbf{f} = \text{MLP}_f(F(\bar{\mathbf{x}}))$ and the signed

distance $d = d_o + \Delta d = d_o + \text{MLP}_d(F(\bar{\mathbf{x}}), d_o)$, where d_o is body SDF queried from SMPL for \mathbf{x} . We then convert the signed distance value d_i of each point \mathbf{x}_i along a ray R to density value σ_i as $\sigma_i = \frac{1}{\alpha} \cdot \text{Sigmoid}(\frac{-d_i}{\alpha})$, where $\alpha > 0$ is a learnable parameter that controls the tightness of the density around the surface boundary. By integration along the ray R we can get the corresponding pixel feature as

$$I(R) = \sum_{i=1}^N \left(\prod_{j=1}^{i-1} e^{-\sigma_j \cdot \delta_j} \right) \cdot (1 - e^{-\sigma_i \cdot \delta_i}) \cdot f_i, \quad (6)$$

where $\delta_i = \|\mathbf{x}_i - \mathbf{x}_{i-1}\|$ and N is number of points sampled per ray. By aggregating all rays, we can get the final image feature which is feed into a super-resolution module [28] to generate the final high-resolution synthesized image.

3.4. Training

We use the non-saturating GAN loss L_{GAN} [28] with R1 regularization L_{Reg} [37] to train our model end-to-end. We also adopt the dual-discriminator proposed by EG3D [2]. It feeds both the rendered raw image and the decoded high-resolution image into the discriminator for improving consistency of the generated multi-view images. Moreover, as observed in [13], most of the human generation artifacts appear in face regions due to low resolution compared with full bodies. Thus, we further enhance the quality of the generated human faces by cropping the head regions and feeding it to an additional discriminator which is jointly trained with the whole framework. For 512^2 resolution image, an 80^2 square covering the whole head region is used. To obtain better controllability, we feed both SMPL parameters \mathbf{p} and camera parameters $\hat{\mathbf{c}}$ as conditions to the discriminator for adversary training. To regularize the learned SDFs, we apply Eikonal loss to the sampled points as:

$$L_{\text{Eik}} = \sum_{\mathbf{x}_i} (|\nabla d_i| - 1)^2, \quad (7)$$

where \mathbf{x}_i and d_i denote the sampled point and predicted signed distance value, respectively. Following [45], we adopt a minimal surface loss to encourage the model to represent human geometry with minimal volume of zero-crossings that penalizes the SDF close to zero: $L_{\text{Minsurf}} = \sum_{\mathbf{x}_i} \exp(-100|d_i|)$. To prevent the learned deformation network from collapsing, we use a deformation regularization loss to regularize the residual deformation $\Delta \bar{\mathbf{x}}_i$ to be small: $L_{\text{Deform}} = \sum_{\mathbf{x}_i} \|\Delta \bar{\mathbf{x}}_i\|$. Along with the geometric prior loss in Eqn. (5), the overall loss is formulated as

$$L_{\text{total}} = L_{\text{GAN}} + \lambda_{\text{Reg}} L_{\text{Reg}} + \lambda_{\text{Eik}} L_{\text{Eik}} + \lambda_{\text{Minsurf}} L_{\text{Minsurf}} + \lambda_{\text{Deform}} L_{\text{Deform}} + \lambda_{\text{Prior}} L_{\text{Prior}}, \quad (8)$$

where λ_* are the corresponding loss weights.

Table 1. **Quantitative comparisons** with baselines on four datasets, with best results in bold.

	MPV				UBC				DeepFashion				SHHQ			
	FID↓	FaceFID↓	Depth↓	PCK↑	FID↓	FaceFID↓	Depth↓	PCK↑	FID↓	FaceFID↓	Depth↓	PCK↑	FID↓	FaceFID↓	Depth↓	PCK↑
StyleNeRF-256 ²	10.71	24.32	1.46	-	20.65	34.30	1.44	-	15.93	29.22	1.43	-	13.52	26.21	1.37	-
StyleSDF-512 ²	43.79	69.71	1.79	-	34.12	39.05	1.80	-	45.06	41.78	1.77	-	43.24	47.46	1.78	-
EG3D-512 ²	15.44	33.98	1.31	-	14.55	20.24	1.28	-	14.36	34.99	1.44	-	9.33	35.10	1.43	-
ENARF-128 ²	75.10	57.64	2.32	58.92	41.75	36.34	2.10	54.40	67.96	51.17	2.57	55.06	73.53	49.35	2.43	53.44
EVA3D-512 ²	-	-	-	-	12.61	-	-	99.17	15.91	-	-	87.50	11.99	-	-	88.95
AvatarGen-512 ²	5.25	6.89	.429	98.79	6.71	8.61	.453	99.38	7.68	8.76	.433	99.24	4.29	4.51	.365	99.49

4. Experiments

We evaluate methods of 3D-aware clothed human generation on four real-world fashion datasets: MPV [11], UBC [68], DeepFashion [35] and SHHQ [14]. They contain single clothed people in each image. Since we focus on foreground human generation, we use a segmentation model [8] to remove irrelevant backgrounds. We adopt an off-the-shelf pose estimator [29] to obtain approximate camera and SMPL parameters. We filter out images with partial observations and those with poor SMPL estimations, and get nearly 13K, 31K, 12K and 39K full-body images for each dataset, respectively. We align and crop images according to the estimated keypoints and scales, and resize them to 512² resolution. We sample 48 points along each ray for volumetric rendering. Horizontal-flip augmentation is used during training. We note that these datasets are primarily composed of front-view images—few images captured from side or back views. To compensate this, we sample more side- and back-view images to re-balance viewpoint distributions following [2]. Our data processing scripts and pre-processed datasets will be released.

4.1. Comparisons

Baselines. We compare AvatarGen against five state-of-the-art methods for 3D-aware image synthesis: EG3D [2], StyleSDF [45], StyleNeRF [17], ENARF-GAN [44] and EVA3D [20]. EG3D and StyleNeRF combine volume renderer with 2D decoder for high-resolution image synthesis. StyleSDF uses SDF for regularized geometry modeling. ENARF-GAN and EVA3D leverage 3D human priors for animatable human generation as well.

Quantitative evaluations. Tab. 1 provides quantitative comparisons between AvatarGen and baselines. We measure image quality with Fréchet Inception Distance (FID) [19] between 50k generated images and all of the available real images. We also evaluate the quality of the generated faces by cropping the face regions (80² for 512²-resolution image) from the generated and real images to compute FaceFID. We evaluate geometry quality by calculating Mean Squared Error (MSE) against pseudo groundtruth (GT) depth-maps (*Depth*) that are estimated from the generated images by [54]. Following [44], we use

Percentage of Correct Keypoints (PCK) to evaluate the effectiveness of the pose controllability. For additional evaluation details, please refer to the appendix. From Tab. 1, we observe our model outperforms all the baselines w.r.t. all the metrics and datasets. Notably, it outperforms baseline models by significant margins (50.9%, 51.1%, 51.7%, 54.0% in FID) on four datasets. These results clearly demonstrate its superiority in clothed human synthesis. Moreover, it maintains state-of-the-art geometry quality and pose accuracy.

Qualitative results. We show a qualitative comparison against baselines in Fig. 3. It can be observed that compared with our method, StyleSDF [45] generate 3D avatar with over-smoothed geometry. In addition, the noises and holes can be observed around the generated avatars and the geometry details like face and clothes are missing. EG3D [2] struggles to learn 3D human geometry from 2D images and suffers degenerated qualities. Although using pose priors for 3D human generations, ENARF-GAN still suffers low rendering quality and undesired geometry. Compared with them, AvatarGen generates 3D-aware avatars with high-fidelity appearances and learns the complex human geometries from 2D images only. Also, AvatarGen can generate avatar in diverse poses with much better geometric details. Please refer to our [project page](#) and Appendix for more results.

4.2. Ablation studies

We conduct ablation studies on DeepFashion (256 × 256) as it contains more diverse appearances and poses.

Geometry proxy. Our AvatarGen uses SDF as geometry proxy to facilitate the geometry learning. To study its effectiveness, we also evaluate our model with density field as the proxy. As shown in Tab. 2a, using the density field degrades quality of the generated avatars significantly—16.8% and 22.0% increases in FID and FaceFID, and 11.6% increase in Depth error. This indicates SDF is important for the model to more precisely represent clothed human geometry, especially for detailed regions like face.

We also show quantitative results of the model trained with density (left) or SDF (right) as geometry proxy in Fig. 4. We observe the model trained with density fields can generate human avatars with reasonable geometry. How-



Figure 3. **Qualitative comparisons** of generation results against baselines including StyleSDF [45], EG3D [2] and ENARF-GAN [44].

Table 2. **Ablation study** on Deepfashion. In (d), *w/o* denotes without using SMPL body priors, *Can.* or *Obs.* means using body SDF priors from canonical or observation spaces, *Obs.+raw* means predicting raw SDFs with priors from observation spaces.

<i>Geo.</i>	FID	FaceFID	Depth
Density	7.87	11.21	.652
SDF	6.54	8.74	.576

(a) The effect of different geometry proxies.

<i>Deform.</i>	FID	FaceFID	Depth
IS	7.89	12.90	.752
IS+RD	6.54	8.74	.576

(b) Deformation schemes.

<i>Face Disc.</i>	FID	FaceFID	Depth
w/o	6.02	12.31	.604
w/	6.54	8.74	.576

(c) The effect of face discriminator.

<i>SDF Scheme</i>	FID	FaceFID	Depth
W/o	7.16	10.63	.689
Can.	7.09	9.27	.592
Obs.+raw	7.03	10.23	.602
Obs.	6.54	8.74	.576

(d) SDF prediction schemes.

<i>Ray Steps</i>	FID	FaceFID	Depth
12	7.76	12.44	.656
24	7.59	12.02	.636
36	7.07	11.30	.626
48	6.54	8.74	.576

(e) Number of ray steps.

<i>KNN</i>	FID	FaceFID	Depth
1	6.54	8.74	.576
2	6.49	9.55	.583
3	6.20	9.72	.578
4	6.17	8.88	.575

(f) KNN in inverse skinning deformation.

ever, it tends to generate noisy body surface. Besides, redundant geometry (*e.g.*, first two examples) is observed in the background regions due to the lack of geometric constraints. Compared with it, the model trained with SDF yields smoother human body surface with better quality thanks to the geometric regularization introduced by SDF.

SDF prediction schemes. AvatarGen predicts residual SDFs of clothed humans on top of the SMPL body mesh. As shown in Tab. 2d, if removing SMPL body guidance and directly predicting residual SDFs (1st row), the performance drops significantly, *i.e.*, 8.7%, 17.8%, 16.4% increase in FID, FaceFID and Depth error. This indicates the coarse SMPL body prior is important for guiding AvatarGen to better generate clothed human geometry. We also compare the performance between SMPL body SDFs queried from observation (*Obs.*) and canonical (*Can.*) spaces. The model guided by the body SDFs queried from *Obs.*, which are more accurate, yielding better performance.

In addition, we study the effect of two SDF prediction schemes—predicting raw SDFs directly (*Obs.+raw*) and predicting SDF residuals on top of the coarse SMPL body from observation space. We see the residual prediction scheme delivers better results as it alleviates the geometry learning difficulties. Moreover, we study the effect of SMPL geometric prior loss in Eqn. (5). Removing it will lead to performance drop w.r.t. all the metrics (FID: 7.20 vs. 6.54, FaceFID: 10.29 vs. 8.74, Depth: 0.645 vs. 0.576), verifying its effectiveness for regularizing geometry learning.

Deformation schemes. Our model uses a pose-guided deformation to un-warp spatial points from the observation space to the canonical space. We also evaluate other two deformation schemes in Tab. 2b: 1) residual deformation [47] only (*RD*), 2) inverse LBS deformation [22] only (*IS*). When using *RD* only, the model training does not converge, indicating that learning deformation implicitly cannot handle large articulation of humans and lead to implausible re-



Figure 4. **Ablation on geometry proxy.** We compare the results of AvatarGen trained with density and signed distance fields.



Figure 5. **Ablation on deformation network.** The visualization of the generated canonical and posed avatars of our model trained with (left) and without (right) deformation fields. Clear artifacts can be observed if we remove the deformation module during model training.

sults. When using IS only, the model achieves a reasonable result (FID: 7.89, FaceFID: 12.9, Depth: 0.752), verifying the importance of the explicitly pose-guided deformation.

Further combining IS and RD (our model) boosts the performance sharply—20.6%, 32.2% and 23.4% decrease in FID, FaceFID and Depth respectively. These results show the

residual deformation, collaborating with the posed-guided inverse LSB transformation, indeed better represents non-rigid clothed human body deformation, yielding better appearance and geometry modeling.

To better study the effects of the proposed deformation network, we visualize generation results (*i.e.*, avatars in the canonical and target observation spaces) of AvatarGen trained with (left) and without (right) it in Fig. 5. From the figure, we observe the deformation network helps to learn better canonical to observation mapping and clearly improves the quality of the generated canonical avatars, and thus lead to high-quality posed avatars generation. Notably, our deformation network can help to build the correct correspondence between the canonical to observation spaces even for loose clothes like dresses.

Face discriminator. Tab. 2c shows the effect of using the face discriminator. We can observe a significant drop in the quality of faces if disable the face discriminator, *i.e.*, 12.31 *vs.* 8.74 in FaceFID. Although the overall FID is slightly improved, the geometry quality becomes worse. This indicates the additional face discriminator is helpful for learning geometry details and improving quality of the target region. Please see qualitative comparisons in Appendix.

Number of ray steps. Tab. 2e shows the effect of the number of points sampled per camera ray. With only 12 sampled points for each ray, AvatarGen already achieves acceptable results, *i.e.*, 7.76, 12.44 and 0.656 in FID, FaceFID and Depth. With more sampling points, the performance monotonically increases, demonstrating the capacity of AvatarGen in 3D-aware human synthesis.

Number of KNN in inverse skinning deformation. For any spatial points, we use Nearest Neighbor to find the corresponding skinning weights for the inverse LBS transformation (Eqn. (2)). Here we study how the number of KNN neighbors affects the model performance in Tab. 2f. We observe that using more KNN neighbors gives slightly better FID performance, but worse geometry and much longer training time as the model need to retrieve more neighbors.

4.3. Applications

Portrait image reconstruction and animation. Fig. 6 shows the application of AvatarGen for single-view 3D reconstruction. Following [56], we fit the target images by optimizing the latent code with MSE loss and perceptual loss to recover both the appearance and geometry. With the recovered 3D representation, we manipulate the images under novel camera poses. Thanks to its disentangled design, AvatarGen also can re-animate the generated avatars with a preserved identity and high-fidelity textures under different poses and shapes specified by the SMPL control signals.

Text-guided synthesis. Recent works [30, 48] have explored using a text-image embedding [53] to guide GANs

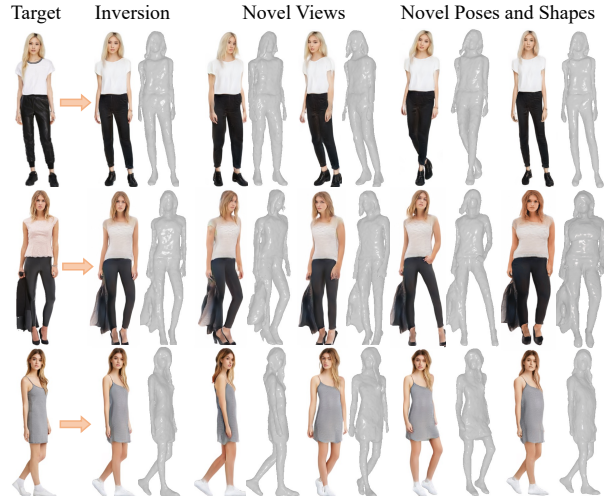


Figure 6. **Portrait image reconstruction and animation** results of AvatarGen. Given target portrait image, we reconstruct 3D-aware appearance and geometry of the human, who is rendered under novel camera views, and re-posed/shaped by taking novel SMPL parameters as control signals and animated accordingly. The model for inversion is trained with DeepFashion and the target images are from SHHQ. Better viewed in 2× zoom.

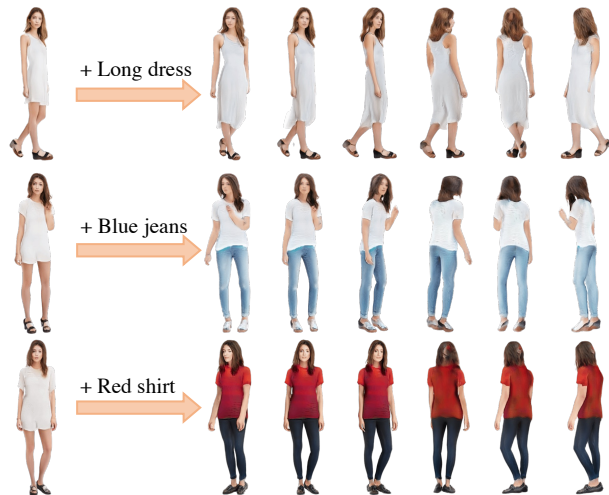


Figure 7. **Text-guided synthesis** results of AvatarGen with multi-view rendering. Different poses and text prompts are used for CLIP-guided optimization. Better viewed in 2× zoom.

for controllable image synthesis. We also visualize text-guided clothed human synthesis in Fig. 7. Specifically, we follow StyleCLIP [48] to optimize the latent code of the synthesized images with a sequence of text prompts that specify different cloth styles. Then we synthesize the re-dressed human avatars under different camera poses.

5. Conclusion

This work introduced the first 3D-aware clothed human avatar generative model, AvatarGen. By factorizing the generative process into the canonical human generation and deformation stages, it can leverage the geometry priors and effective tri-plane representation to address the challenges in animatable human avatar generation. We demonstrated it can generate high-fidelity humans with disentangled geometry controllability, and support several downstream applications. We believe our method will make the creation of human avatars more accessible to ordinary users, assist designers and reduce the manual cost.

Limitations. We presented a high-fidelity animatable 3D human GAN, but there is still space for further improvement in our method. 1) It relies on the SMPL estimations. Inaccurate estimations would lead to generation quality degradation. 2) The fine-grained motions of the human avatars generated by our method, like face expression changes, cannot be controlled yet. Using more expressive 3D human model, e.g., SMPL-X as guidance would be a promising solution.

References

- [1] Panos Achlioptas, Olga Diamanti, Ioannis Mitliagkas, and Leonidas Guibas. Learning representations and generative models for 3d point clouds. In *ICML*, 2018. 2
- [2] Eric R Chan, Connor Z Lin, Matthew A Chan, Koki Nagano, Boxiao Pan, Shalini De Mello, Orazio Gallo, Leonidas Guibas, Jonathan Tremblay, Sameh Khamis, et al. Efficient geometry-aware 3d generative adversarial networks. *CVPR*, 2022. 2, 3, 4, 5, 6, 7, 13, 19
- [3] Eric R Chan, Marco Monteiro, Petr Kellnhofer, Jiajun Wu, and Gordon Wetzstein. pi-gan: Periodic implicit generative adversarial networks for 3d-aware image synthesis. In *CVPR*, 2021. 2
- [4] Jianchuan Chen, Ying Zhang, Di Kang, Xuefei Zhe, Linchao Bao, Xu Jia, and Huchuan Lu. Animatable neural radiance fields from monocular rgb videos. *arXiv*, 2021. 3, 4
- [5] Mingfei Chen, Jianfeng Zhang, Xiangyu Xu, Lijuan Liu, Yujun Cai, Jiashi Feng, and Shuicheng Yan. Geometry-guided progressive nerf for generalizable and efficient neural human rendering. *arXiv*, 2021. 2, 3
- [6] Zhiqin Chen and Hao Zhang. Learning implicit fields for generative shape modeling. In *CVPR*, 2019. 2
- [7] Alvaro Collet, Ming Chuang, Pat Sweeney, Don Gillett, Dennis Evseev, David Calabrese, Hugues Hoppe, Adam Kirk, and Steve Sullivan. High-quality streamable free-viewpoint video. In *ACM Trans. on Graphics*, 2015. 2, 3
- [8] PaddlePaddle Contributors. Paddleseg, end-to-end image segmentation kit based on paddlepaddle. <https://github.com/PaddlePaddle/PaddleSeg>, 2019. 6
- [9] Paul Debevec, Tim Hawkins, Chris Tchou, Haarm-Pieter Duiker, Westley Sarokin, and Mark Sagar. Acquiring the reflectance field of a human face. In *Computer graphics and interactive techniques*, 2000. 2, 3
- [10] Yu Deng, Jiaolong Yang, Jianfeng Xiang, and Xin Tong. Gram: Generative radiance manifolds for 3d-aware image generation. *CVPR*, 2022. 2
- [11] Haoye Dong, Xiaodan Liang, Xiaohui Shen, Bochao Wang, Hanjiang Lai, Jia Zhu, Zhiting Hu, and Jian Yin. Towards multi-pose guided virtual try-on network. In *ICCV*, 2019. 6, 18
- [12] Mingsong Dou, Sameh Khamis, Yury Degtyarev, Philip Davidson, Sean Ryan Fanello, Adarsh Kowdle, Sergio Orts Escolano, Christoph Rhemann, David Kim, Jonathan Taylor, et al. Fusion4d: Real-time performance capture of challenging scenes. In *ACM Trans. on Graphics*, 2016. 2, 3
- [13] Anna Frühstück, Krishna Kumar Singh, Eli Shechtman, Niloy J. Mitra, Peter Wonka, and Jingwan Lu. Insetgan for full-body image generation. In *CVPR*, 2022. 5
- [14] Jianglin Fu, Shikai Li, Yuming Jiang, Kwan-Yee Lin, Chen Qian, Chen-Change Loy, Wayne Wu, and Ziwei Liu. Stylegan-human: A data-centric odyssey of human generation. *arXiv*, 2022. 6, 18
- [15] Thiago L. Gomes, Thiago M. Coutinho, Rafael Azevedo, Renato Martins, and Erickson R. Nascimento. Creating and reenacting controllable 3d humans with differentiable rendering. In *WACV*, 2022. 3
- [16] Ian Goodfellow, Jean Pouget-Abadie, Mehdi Mirza, Bing Xu, David Warde-Farley, Sherjil Ozair, Aaron Courville, and Yoshua Bengio. Generative adversarial nets. In *NeurIPS*, 2014. 2
- [17] Jiatao Gu, Lingjie Liu, Peng Wang, and Christian Theobalt. Stylenerf: A style-based 3d-aware generator for high-resolution image synthesis. *CVPR*, 2022. 2, 4, 6
- [18] Kaiwen Guo, Peter Lincoln, Philip Davidson, Jay Busch, Xueming Yu, Matt Whalen, Geoff Harvey, Sergio Orts-Escolano, Rohit Pandey, Jason Dourgarian, et al. The re-lightables: Volumetric performance capture of humans with realistic relighting. In *ACM Trans. on Graphics*, 2019. 3
- [19] Martin Heusel, Hubert Ramsauer, Thomas Unterthiner, Bernhard Nessler, and Sepp Hochreiter. Gans trained by a two time-scale update rule converge to a local nash equilibrium. *NeurIPS*, 2017. 6
- [20] Fangzhou Hong, Zhaoxi Chen, Yushi Lan, Liang Pan, and Ziwei Liu. Eva3d: Compositional 3d human generation from 2d image collections. *arXiv*, 2022. 3, 6
- [21] Fangzhou Hong, Mingyuan Zhang, Liang Pan, Zhongang Cai, Lei Yang, and Ziwei Liu. Avatarclip: Zero-shot text-driven generation and animation of 3d avatars. *ACM Trans. on Graphics*, 2022. 2
- [22] Zeng Huang, Yuanlu Xu, Christoph Lassner, Hao Li, and Tony Tung. Arch: Animatable reconstruction of clothed humans. In *CVPR*, 2020. 2, 4, 7
- [23] Alec Jacobson, Ilya Baran, Ladislav Kavan, Jovan Popović, and Olga Sorkine. Fast automatic skinning transformations. *ACM Trans. on Graphics*, 2012. 4
- [24] Boyi Jiang, Yang Hong, Hujun Bao, and Juyong Zhang. Selfrecon: Self reconstruction your digital avatar from monocular video. In *CVPR*, 2022. 2
- [25] Tero Karras, Timo Aila, Samuli Laine, and Jaakko Lehtinen. Progressive growing of GANs for improved quality, stability, and variation. In *ICCV*, 2018. 2

- [26] Tero Karras, Miika Aittala, Samuli Laine, Erik Härkönen, Janne Hellsten, Jaakko Lehtinen, and Timo Aila. Alias-free generative adversarial networks. In *NeurIPS*, 2021. 2
- [27] Tero Karras, Samuli Laine, and Timo Aila. A style-based generator architecture for generative adversarial networks. In *CVPR*, 2019. 2
- [28] Tero Karras, Samuli Laine, Miika Aittala, Janne Hellsten, Jaakko Lehtinen, and Timo Aila. Analyzing and improving the image quality of StyleGAN. In *CVPR*, 2020. 2, 4, 5, 13
- [29] Muhammed Kocabas, Chun-Hao P Huang, Otmar Hilliges, and Michael J Black. Pare: Part attention regressor for 3d human body estimation. In *ICCV*, 2021. 3, 6
- [30] Gihyun Kwon and Jong Chul Ye. Clipstyler: Image style transfer with a single text condition. In *CVPR*, 2022. 9
- [31] Ruihui Li, Xianzhi Li, Chi-Wing Fu, Daniel Cohen-Or, and Pheng-Ann Heng. Pu-gan: a point cloud upsampling adversarial network. In *ICCV*, 2019. 2
- [32] Yiyi Liao, Katja Schwarz, Lars Mescheder, and Andreas Geiger. Towards unsupervised learning of generative models for 3D controllable image synthesis. In *CVPR*, 2020. 2
- [33] Lingjie Liu, Marc Habermann, Viktor Rudnev, Kripasindhu Sarkar, Jiatao Gu, and Christian Theobalt. Neural actor: Neural free-view synthesis of human actors with pose control. *ACM Trans. on Graphics*, 2021. 3, 4
- [34] Ting Liu, Jianfeng Zhang, Xuecheng Nie, Yunchao Wei, Shikui Wei, Yao Zhao, and Jiashi Feng. Spatial-aware texture transformer for high-fidelity garment transfer. In *IEEE Trans. on Image Processing*, 2021. 2
- [35] Ziwei Liu, Ping Luo, Shi Qiu, Xiaogang Wang, and Xiaoou Tang. Deepfashion: Powering robust clothes recognition and retrieval with rich annotations. In *CVPR*, 2016. 6, 18
- [36] Matthew Loper, Naureen Mahmood, Javier Romero, Gerard Pons-Moll, and Michael J Black. Smpl: A skinned multi-person linear model. *ACM Trans. on Graphics*, 2015. 2, 3
- [37] Lars Mescheder, Andreas Geiger, and Sebastian Nowozin. Which training methods for gans do actually converge? In *ICML*, 2018. 5
- [38] Lars Mescheder, Michael Oechsle, Michael Niemeyer, Sebastian Nowozin, and Andreas Geiger. Occupancy networks: Learning 3d reconstruction in function space. In *CVPR*, 2019. 2
- [39] Ben Mildenhall, Pratul P Srinivasan, Matthew Tancik, Jonathan T Barron, Ravi Ramamoorthi, and Ren Ng. Nerf: Representing scenes as neural radiance fields for view synthesis. In *ECCV*, 2020. 2, 3
- [40] Thu Nguyen-Phuoc, Chuan Li, Lucas Theis, Christian Richardt, and Yong-Liang Yang. HoloGAN: Unsupervised learning of 3D representations from natural images. In *ICCV*, 2019. 2
- [41] Thu Nguyen-Phuoc, Christian Richardt, Long Mai, Yong-Liang Yang, and Niloy Mitra. BlockGAN: Learning 3D object-aware scene representations from unlabelled images. In *NeurIPS*, 2020. 2
- [42] Michael Niemeyer and Andreas Geiger. Giraffe: Representing scenes as compositional generative neural feature fields. In *CVPR*, 2021. 2, 4
- [43] Atsuhiko Noguchi, Xiao Sun, Stephen Lin, and Tatsuya Harada. Neural articulated radiance field. In *ICCV*, 2021. 2
- [44] Atsuhiko Noguchi, Xiao Sun, Stephen Lin, and Tatsuya Harada. Unsupervised learning of efficient geometry-aware neural articulated representations. In *ECCV*, 2022. 3, 6, 7, 19
- [45] Roy Or-El, Xuan Luo, Mengyi Shan, Eli Shechtman, Jeong Joon Park, and Ira Kemelmacher-Shlizerman. Stylesdf: High-resolution 3d-consistent image and geometry generation. *CVPR*, 2022. 2, 3, 4, 5, 6, 7, 19
- [46] Jeong Joon Park, Peter Florence, Julian Straub, Richard Newcombe, and Steven Lovegrove. Deepsdf: Learning continuous signed distance functions for shape representation. In *CVPR*, 2019. 2
- [47] Keunhong Park, Utkarsh Sinha, Jonathan T Barron, Sofien Bouaziz, Dan B Goldman, Steven M Seitz, and Ricardo Martin-Brualla. Nerfies: Deformable neural radiance fields. In *ICCV*, 2021. 4, 7
- [48] Or Patashnik, Zongze Wu, Eli Shechtman, Daniel Cohen-Or, and Dani Lischinski. Styleclip: Text-driven manipulation of stylegan imagery. In *ICCV*, 2021. 9
- [49] Sida Peng, Junting Dong, Qianqian Wang, Shangzhan Zhang, Qing Shuai, Hujun Bao, and Xiaowei Zhou. Animatable neural radiance fields for human body modeling. *ICCV*, 2021. 2, 3, 4
- [50] Sida Peng, Shangzhan Zhang, Zhen Xu, Chen Geng, Boyi Jiang, Hujun Bao, and Xiaowei Zhou. Animatable neural implicit surfaces for creating avatars from videos. *arXiv*, 2022. 2, 3, 4, 5
- [51] Sida Peng, Yuanqing Zhang, Yinghao Xu, Qianqian Wang, Qing Shuai, Hujun Bao, and Xiaowei Zhou. Neural body: Implicit neural representations with structured latent codes for novel view synthesis of dynamic humans. In *CVPR*, 2021. 3
- [52] Albert Pumarola, Enric Corona, Gerard Pons-Moll, and Francesc Moreno-Noguer. D-nerf: Neural radiance fields for dynamic scenes. In *CVPR*, 2021. 4
- [53] Alec Radford, Jong Wook Kim, Chris Hallacy, Aditya Ramesh, Gabriel Goh, Sandhini Agarwal, Girish Sastry, Amanda Askell, Pamela Mishkin, Jack Clark, et al. Learning transferable visual models from natural language supervision. In *ICML*, 2021. 9
- [54] Shunsuke Saito, Tomas Simon, Jason Saragih, and Hanbyul Joo. Pifuhd: Multi-level pixel-aligned implicit function for high-resolution 3d human digitization. In *CVPR*, 2020. 6
- [55] Katja Schwarz, Yiyi Liao, Michael Niemeyer, and Andreas Geiger. Graf: Generative radiance fields for 3d-aware image synthesis. *NeurIPS*, 2020. 2
- [56] Guoxian Song, Linjie Luo, Jing Liu, Wan-Chun Ma, Chunpong Lai, Chuanxia Zheng, and Tat-Jen Cham. Agilegan: stylizing portraits by inversion-consistent transfer learning. *ACM Trans. on Graphics*, 2021. 9
- [57] Shih-Yang Su, Frank Yu, Michael Zollhöfer, and Helge Rhodin. A-nerf: Articulated neural radiance fields for learning human shape, appearance, and pose. In *NeurIPS*, 2021. 3

- [58] Zhuo Su, Lan Xu, Zerong Zheng, Tao Yu, Yebin Liu, and Lu Fang. Robustfusion: Human volumetric capture with data-driven visual cues using a rgbd camera. In *ECCV*, 2020. 2, 3
- [59] Attila Szabó, Givi Meishvili, and Paolo Favaro. Unsupervised generative 3D shape learning from natural images. *arXiv*, 2019. 2
- [60] Peng Wang, Lingjie Liu, Yuan Liu, Christian Theobalt, Taku Komura, and Wenping Wang. Neus: Learning neural implicit surfaces by volume rendering for multi-view reconstruction. *NeurIPS*, 2021. 2, 4
- [61] Chung-Yi Weng, Brian Curless, Pratul P. Srinivasan, Jonathan T. Barron, and Ira Kemelmacher-Shlizerman. HumanNeRF: Free-viewpoint rendering of moving people from monocular video. *CVPR*, 2022. 3
- [62] Jiajun Wu, Chengkai Zhang, Tianfan Xue, William T. Freeman, and Joshua B. Tenenbaum. Learning a probabilistic latent space of object shapes via 3D generative-adversarial modeling. In *NeurIPS*, 2016. 2
- [63] Donglai Xiang, Fabian Prada, Timur Bagautdinov, Weipeng Xu, Yuan Dong, He Wen, Jessica Hodgins, and Chenglei Wu. Modeling clothing as a separate layer for an animatable human avatar. *ACM Trans. on Graphics*, 2021. 2
- [64] Hongyi Xu, Thiemo Alldieck, and Cristian Sminchisescu. H-nerf: Neural radiance fields for rendering and temporal reconstruction of humans in motion. *NeurIPS*, 2021. 2, 3, 4
- [65] Xiangyu Xu and Chen Change Loy. 3D human texture estimation from a single image with transformers. In *ICCV*, 2021. 3
- [66] Yang Xue, Yuheng Li, Krishna Kumar Singh, and Yong Jae Lee. Giraffe hd: A high-resolution 3d-aware generative model. In *CVPR*, 2022. 2
- [67] Lior Yariv, Jiatao Gu, Yoni Kasten, and Yaron Lipman. Volume rendering of neural implicit surfaces. In *NeurIPS*, 2021. 2, 4
- [68] Polina Zablotkaia, Aliaksandr Siarohin, Bo Zhao, and Leonid Sigal. Dwnet: Dense warp-based network for pose-guided human video generation. *BMVC*, 2019. 6, 18
- [69] Jiakai Zhang, Xinhang Liu, Xinyi Ye, Fuqiang Zhao, Yanshun Zhang, Minye Wu, Yingliang Zhang, Lan Xu, and Jingyi Yu. Editable free-viewpoint video using a layered neural representation. *ACM Trans. on Graphics*, 2021. 2
- [70] Jichao Zhang, Enver Sangineto, Hao Tang, Aliaksandr Siarohin, Zhun Zhong, Nicu Sebe, and Wei Wang. 3d-aware semantic-guided generative model for human synthesis. In *ECCV*, 2022. 2
- [71] Jiakai Zhang, Liao Wang, Xinhang Liu, Fuqiang Zhao, Minzhang Li, Haizhao Dai, Boyuan Zhang, Wei Yang, Lan Xu, and Jingyi Yu. Neuvv: Neural volumetric videos with immersive rendering and editing. *ACM Trans. on Graphics*, 2022. 2

We provide more implementation details in Section A. We present additional baseline comparisons, ablation studies and more visual results in Section B. For the results in video format, please refer to the [project page](#).

A. Implementation Details

We detail the implementation of each module of AvatarGen and the hyper-parameter choice in this section.

Backbone. We adopt the StyleGAN2 [28] backbone as tri-plane generator and two blocks of StyleGAN2-modulated convolutional layers as super-resolution module, following EG3D [2]. The output tri-plane resolution is set as 256×256 with 96 channels which are then split to three planes for feature sampling. We use the MLP-based mapping network in StyleGAN2 to encode the latent code and camera condition. We adopt a similar dual-discriminator architecture used in EG3D for regularizing the generator training. Different from EG3D, we further feed an additional upsampled image of the head region to the discriminator to improve the generation quality of human faces. For 512^2 -resolution image, an 80^2 -squared image covering the whole head region is cropped for face discrimination.

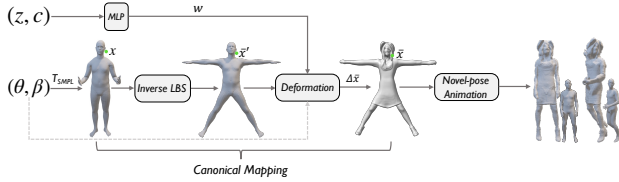


Figure S8. Detailed architecture of our canonical mapping.

Canonical mapping. Fig S8 shows details of the canonical mapping module. For a point \mathbf{x}_i , we first find its nearest point \mathbf{v}^* on the SMPL body surface: $\mathbf{v}^* = \arg \min_{\mathbf{v} \in \mathcal{V}} \|\mathbf{x}_i - \mathbf{v}\|_2$. Then, we use its corresponding skinning weights \mathbf{s}^* to deform \mathbf{x}_i to $\bar{\mathbf{x}}'_i$ in the canonical space as:

$$\bar{\mathbf{x}}'_i = T_o(\mathbf{x}_i | \mathbf{p}) = T_{IS}(\mathbf{x}_i, \mathbf{s}^*, \mathbf{p}). \quad (9)$$

For the fine-grained geometric deformation, we further train a deformation network to learn a residual deformation:

$$\Delta \bar{\mathbf{x}}_i = \text{MLPs}(\text{Concat}[\text{Embed}(\mathbf{x}_i), \mathbf{w}, \mathbf{p}]), \quad (10)$$

where \mathbf{w} is the latent style code mapped from the input latent code \mathbf{z} via MLP, which contains appearance and geometric details of the current generation. We concatenate it with the position-embedded \mathbf{x}_i and SMPL \mathbf{p} and feed them to MLPs to yield the residual deformation $\Delta \bar{\mathbf{x}}_i$. Thus, the final canonical mapping T is formulated as

$$\bar{\mathbf{x}}_i = T(\mathbf{x}_i) = \bar{\mathbf{x}}'_i + \Delta \bar{\mathbf{x}}_i. \quad (11)$$

During inference, given the latent code \mathbf{z} and camera \mathbf{c} , AvatarGen leverages the pre-trained tri-plane to synthesize the corresponding appearance and geometry of the canonical avatar, and then animate it by deforming the canonical one according to the desired SMPL control signals.

SDF-based volume renderer. The detailed architecture of our SDF-based volume renderer is shown in Fig. S9. For any sampled points \mathbf{x} on the rays, we first un-warp it to $\bar{\mathbf{x}}$ by canonical mapping (Fig. S8). We query feature $F(\bar{\mathbf{x}})$ for $\bar{\mathbf{x}}$ from the canonical tri-plane, and feed it into two MLPs to predict the color feature $\mathbf{f} = \text{MLP}_f(F(\bar{\mathbf{x}}))$ and the signed distance $d = d_o + \Delta d = d_o + \text{MLP}_d(F(\bar{\mathbf{x}}), d_o)$, where d_o is body SDF queried from SMPL for \mathbf{x} . We then convert the signed distance value d_i of each point \mathbf{x}_i along a ray R to density value σ_i as $\sigma_i = \frac{1}{\alpha} \cdot \text{Sigmoid}(\frac{-d_i}{\alpha})$, where $\alpha > 0$ is a learnable parameter that controls the tightness of the density around the surface boundary. By integration along the ray R we can get the corresponding pixel feature as

$$I(R) = \sum_{i=1}^N \left(\prod_{j=1}^{i-1} e^{-\sigma_j \cdot \delta_j} \right) \cdot (1 - e^{-\sigma_i \cdot \delta_i}) \cdot \mathbf{f}_i, \quad (12)$$

where $\delta_i = \|\mathbf{x}_i - \mathbf{x}_{i-1}\|$ and N is number of points sampled per ray. By aggregating all rays, we can get the high-dimensional feature image for the following super-resolution module.

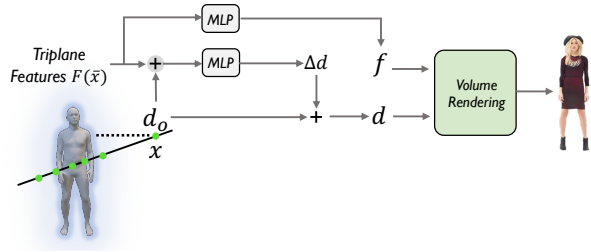


Figure S9. Detailed architecture of SDF-based volume renderer.

Hyper-parameter. The learning rate is set as 2.5×10^{-3} for generator and 2×10^{-3} for discriminator. For loss function, we set $\lambda_{\text{Reg}} = 10$, $\lambda_{\text{Eik}} = 10^{-3}$, $\lambda_{\text{Minsurf}} = 0.05$, $\lambda_{\text{Deform}} = 10$, $\lambda_{\text{Prior}} = 1$. The model is trained on 8 NVIDIA V100 GPUs with batch size of 16. Similar to EG3D, we adopt a progressive growing strategy, *i.e.*, we first train the model with 64^2 -resolution volume rendering and then progressively grow it to 128^2 -resolution. The total training process takes about 4 days to converge.

B. More results

B.1. Face discriminator

We show the comparison of our model trained with and without face discrimination in Fig. S10. We can observe

that our proposed face discrimination clearly improves the quality of the face region. If we disable the face discrimination, the model tends to produce distorted faces especially when rendered from different camera poses.

B.2. Disentanglement between geometry and appearance

In Fig. S11, we visualize more synthesized human avatars with the same pose and shape conditions but different latent codes. We observe AvatarGen can synthesize diverse avatars with the desired shape and pose as specified by the input SMPL signals. This clearly demonstrates the proposed decomposed pipeline can well disentangle geometry generation from appearance, making animatable avatar generation possible.

B.3. Comparison with 2D GAN

We show the comparison of 2D StyleGAN2 with our generation results in Fig S12. Both models are trained on DeepFashion with 512² resolution. Although the FID of StyleGAN2 is much lower than ours (*i.e.*, 3.07 vs. 7.68), it is difficult for StyleGAN2 to capture the structure of human body and thus suffers from the artifacts of unnatural poses and distorted body parts. Our method, however, with the geometry priors and learned 3D-aware representation, can effectively capture the structure of human body and generate high-quality images given the desired condition.

B.4. More visualization results

We show more visualization results of our method in Fig. S13 and Fig. S14, as well as multi-view rendering results of baseline methods on Fig. S15. Please visit our [project page](#) for results in video format.



Figure S10. Ablation on face discrimination, the result generated by our model with face discrimination is shown on the left side and the result without face discrimination is shown on the right side. Multi-view rendering of both geometry and appearance are listed. Face regions are cropped and zoomed in for better visualization.

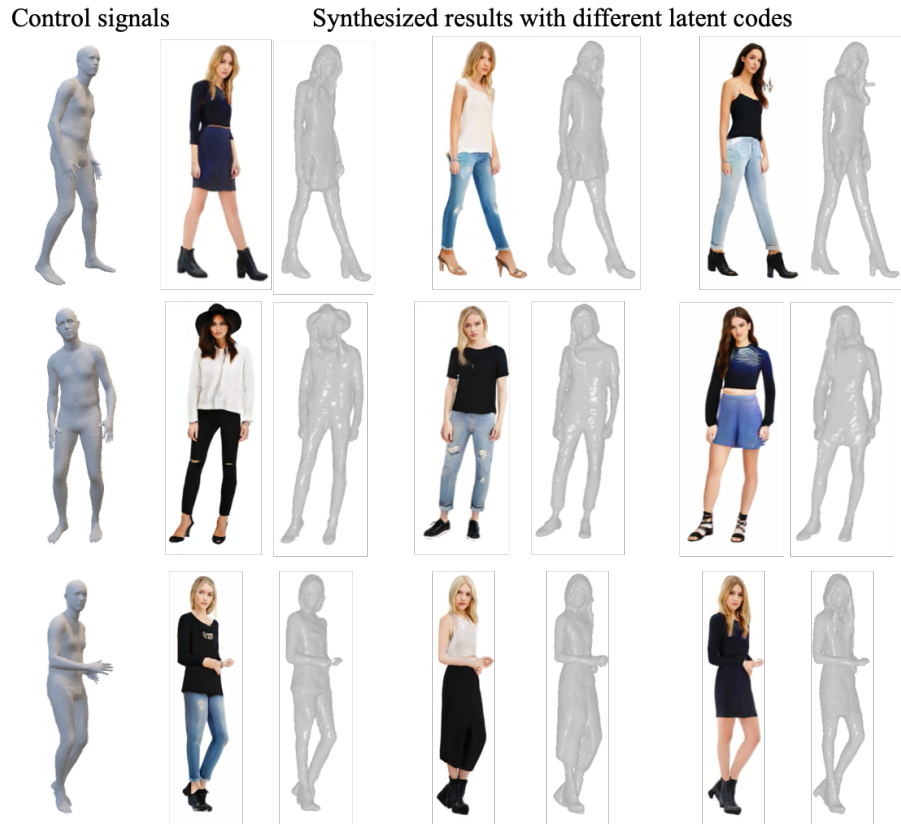


Figure S11. Avatar generated under the same SMPL condition but different latent codes.



Figure S12. Comparison of 2D StyleGAN2 with our AvatarGen.



Figure S13. More multi-view rendering and novel pose/shape synthesis results. Best viewed in 2× zoom.



Figure S14. More multi-view rendering results of AvatarGen on four datasets including DeepFashion [35], UBCFashion [68], MPV [11] and SHHQ [14].



Figure S15. More multi-view rendering results of baseline methods: StyleSDF [45], EG3D [2] and ENARF [44].